# Fault Characteristic Analysis of a Rubbing Rotor in the Presence of Pedestal Looseness

Hui Ma[1, 2*], Xinxing Ma[1], Qingkai Han[3], Bangchun Wen[1]

1 School of Mechanical Engineering & Automation, Northeastern University, Shenyang, Liaoning 110819, P R China

2 State Key Laboratory for Strength and Vibration of Mechanical Structures, Xi'an Jiaotong University, Xi'an 710049, P R China

3 School of Mechanical Engineering, Dalian University of Technology, Dalian, Liaoning 116023, P R China

**Abstract**: Rotor-stator rubbing and pedestal looseness are two of the most common faults in rotating machinery. Researchers have mostly studied the vibration behavior of a rotor with single rotor-stator rubbing or pedestal looseness separately. However, once the pedestal looseness is developed in a rotor, the rotor is more prone to make contact with stator under tight clearance conditions due to increased vibration level. The present research aims to study fault characteristics of the rubbing rotor in the presence of other common rotor faults such as pedestal looseness. The numerical simulation for vibration response of the rubbing rotor system with pedestal looseness fault is carried out and steady-state vibration analysis is presented based on the finite element method (FEM) and contact dynamic theory. The effects of the rotational speed and the stiffness of non-loosened bolts on the dynamic characteristics of the system are discussed. The study concludes that the system motions with both the rubbing and the pedestal looseness are different from those of the rubbing rotor system at some rotating speeds. When the pedestal vibration displacement becomes smaller than the looseness clearance, with the changes of the stiffness of non-loosened bolts, multiple harmonic components such as 2×, 3×, 4×, etc, appear, the amplitude of 4× is second to that of 1× and the vibration displacement decreases at the rubbing location while vibration displacement increases at the pedestal looseness location at the first critical speed. When the pedestal vibration displacement is greater than the looseness clearance, the vibration characteristic of the system is almost the same and the higher harmonics with continuous spectra at looseness location can be observed at the first critical speed. These features can be exploited for the diagnosis of a rubbing rotor system with pedestal looseness fault.

**Keywords:** Pedestal looseness; rubbing; finite element; a rotor system; fault characteristic

* Corresponding author (mahui_2007@163.com)


ISSN 2572-4975 (Print), 2572-4991 (Online)

## 1 Introduction

In a rotor-bearing system, the loosened bolt on the pedestal will reduce the pedestal stiffness and the mechanical damping, and finally results in the violent vibration of the whole system. Especially, the serious looseness fault may induce other faults such as rub-impact fault between the rotor and the stator. It may even lead to disastrous accidents. Therefore, the research on the rubbing fault characteristics of the rotor system in the presence of pedestal looseness is significant in engineering practice for the safe operation of rotating machinery, the extension of its service life and the improvement of its work efficiency.

In the last decades, dynamics of rotor systems with the pedestal looseness and the rotor-stator rubbing fault have attracted the attention of many researchers and many results have been obtained. With reference to the pedestal looseness fault, Muszynska [1,2] presented an analytical, numerical, and experimental simulation of unbalanced rotor-bearing-stator systems with joint looseness or rubbing. Their numerical results contained the synchronous and subsynchronous fractional components of the response, which were verified by experiments. In addition, Chu et al. [3] analyzed vibration characteristics of a rotor-bearing system with the pedestal looseness by establishing a non-linear mathematical model. Stability of these periodic solutions was discussed by using the shooting method and the Floquet theory. When the rotational speed and imbalance of rotors varied, periodic, quasi-periodic and chaotic motions could be observed and three kinds of routes to or out of chaos were found. Using the nonlinear bearing pedestal model simulated by a non-linear spring and a linear damping, Ji et al. [4] analyzed the free and the forced vibration of a non-linear bearing system to illustrate the non-linear effect on the free and forced vibrations by the method of multiple scales. Ma et al. [5] presented a finite element model of a rotor system with pedestal looseness stemming from a loosened bolt and analyzed the effects of the looseness parameters on its dynamic characteristics.

With regards to the rotor-stator rubbing fault, Ehrich [6] found the 8th and 9th order subharmonic vibration responses considering the ideal collision conditions in a high speed rotor of aircraft gas turbine engine. Based on a Jeffcott model, Childs [7] explained 1/2 speed and 1/3 speed whirling motion occurring in rotors which were subject to periodic normal loose or normal-tight radial stiffness variations. Zhang et al. [8] presented a rub-impact micro-rotor model with scaling nonlinear rub-impact force and the nonlinear dynamic characteristics of micro-electro-mechanical systems (MEMS) were investigated when the rotational speed, imbalance, damping coefficient, scale length, and fractal dimension were regarded as the control parameters. Chu et al. [9] investigated periodic, quasi-periodic and chaotic motion of a Jeffcott rotor system with rub-impact fault based on chaos and bifurcation theories. Popprath et al. [10] presented a mathematical model to investigate the dynamics of a Jeffcott-rotor having intermittent contact with a stator. In this model, the nonlinear contact forces of the rotor and the stator are generated by a contact model consisting of contact stiffness, damping and friction.

The above-mentioned research on rotor systems with the rubbing fault are all based on the lumped mass model of the rotor, which is useful for qualitative analyses. With the development of the finite element (FE), many researchers have employed the FE method (FEM) to establish the rotor model [11-15]. In recent years, rotor-stator rubbing simulated by combining the FEM with the nonlinear contact theory has been investigated widely. Based on the nonlinear FEM, Chen et al. [16] investigated the nonlinear transient response due to the rotor-stator contact using the FEM and developed a local contact element. The results demonstrated that four different motions appeared under different conditions; moreover, the rotating speed, friction coefficient and stator stiffness had a great effect on system responses. Chavez et al. [17] adapted a rigid contact model to model the impact between rotor and auxiliary bearing. A unilateral contact is used to simulate the rubbing process and Poisson's impact law to simulate the change of the velocity in the normal direction. By constraints between contact forces and relative kinematics, the evaluation of the mechanical impact dynamics is performed. Ginzinger et al. [18, 19] developed a simulation environment for rotor dynamical problems. Additionally, he simulated the contact between rotor and auxiliary bearing by using unilateral and bilateral constraints, and used Coulomb's friction law to simulate tangential frictional contact. Sahinkaya et al. [20] utilized constrained Lagrangian equations of motion to develop a computationally efficient method to model contact dynamics. This method does not require a direct physical modeling of contact forces. It can be applied to multi-contact cases and is also capable of detecting and simulating the destructive backward whirl rolling motion. Roques et al. [21,22] presented a rotor-stator model of a turbogenerator and investigated rotor-to-stator rubbing caused by an accidental blade-off imbalance. They model the rotor system using the FEM, simulate rotor-to-stator rubbing using the node-to-line contact and solve the highly nonlinear equations due to contact conditions through an explicit prediction-correction time-marching procedure combined with the Lagrange multiplier approach.

Researchers have frequently studied the vibration behavior of a rotor with single faults, such as pedestal looseness, rotor crack and rotor-stator rubbing, etc. However, once the pedestal looseness or rotor crack is developed in a rotor, the rotor is more likely to make contact with stator under tight clearance conditions due to increased vibration level. Patel et al. [23] analyzed the response characteristics of a rotor system with rubbing and crack. Chen et al. [24] established a detailed model of ball bearings in an aeroengine rotor system and analyzed nonlinear characteristics of this system with both imbalance and rub-impact faults.

It is clear the studies on rubbing fault characteristics under the pedestal looseness condition are not sufficient based on the above literature review. In our study, based on the FEM, a pedestal looseness fault model and a rubbing model between the rotor and the stator are proposed firstly. The pedestal looseness fault is simulated by using piecewise linear stiffness and damping models and the rub-impact fault by a fixed point-point contact model. Then by applying the augmented Lagrangian method to deal with contact constraint conditions and the coulomb friction model to simulate rotor-stator frictional characteristics, the dynamics model of rotor system with two faults is established. And the fault characteristics of the rubbing rotor system in the presence of pedestal looseness are analyzed at different rotating speeds and the stiffness of non-loosed bolts, respectively.


ISSN 2572-4975 (Print), 2572-4991 (Online)

This paper consists of four sections. After this introduction, dynamic model of a rotor-bearing system with rubbing fault in the presence of pedestal looseness is established in Section 2, including an equivalent stiffness model of a loosened pedestal in Section 2.1, a rotor-stator fixed-point rubbing model in Section 2.2, and finite element model of the rubbing rotor system in the presence of pedestal looseness in Section 2.3. In Section 3, fault characteristics of the rotor system with rubbing fault in the presence of pedestal looseness are analyzed, and the effects of the rotating speed, the stiffness of non-loosened bolt are discussed in Sections 3.1, 3.2 and 3.3 respectively. Finally, conclusions are given in Section 4.

## 2 Dynamic model of a rotor-bearing system with rubbing fault in the presence of pedestal looseness

In order to efficiently research this system, FE model of rotor-bearing system is simplified according to the following assumptions:

(a) The shaft and discs can be simulated by a Timoshenko beam and the element model is shown in Fig. 1. In the figure, $x$, $y$, $z$ and $\theta_x$, $\theta_y$, $\theta_z$ denote displacements in translation directions and angular displacements in rotation directions, subscripts $A$ and $B$ denote nodes $A$ and $B$ respectively;

(b) For the sliding bearing, the oil-film commonly provides nonlinear elastic and damping forces, but in most cases, the oil-film force can be simplified as linear elastic and damping forces when the journal is apart from the balance position slightly. In such a case, the bearing can be modelled as a stiffness-damping form; stiffness, cross stiffness and damping and cross damping coefficients in horizontal ($z$-coordinate) and vertical ($y$-coordinate) directions should be considered. In this paper, in order to simplify the modelling process of the rotor-bearing system and shorten the FE simulation time, the cross terms are neglected, and the left and right bearings are simulated ideally by identical linear stiffness and damping in $y$ and $z$ directions;

(c) The pedestal looseness is located in the right bearing position and the stiffness and damping between the pedestal and the base are only considered in $y$ direction, namely preload direction of the bolts. Furthermore, only vibration characteristics of the rotor system in pedestal looseness direction are analysed;

(d) The early rubbing is a fixed-point rotor-stator contact and the contact time is very short, thermal effects and friction torque during the rubbing between the rotor and the stator are not considered, and only transverse motion of the rotor is considered.

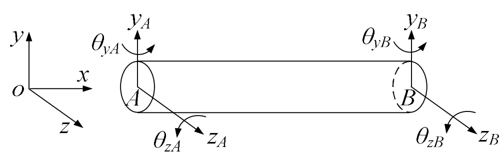


**Fig. 1.** Finite element model of shaft section element

Neglecting axial displacement and corresponding torsional deformation, the general displacement vector of a beam element for the shaft or discs is given as

$$\boldsymbol{u}_s = \begin{bmatrix} y_A & z_A & \theta_{yA} & \theta_{zA} & y_B & z_B & \theta_{yB} & \theta_{zB} \end{bmatrix}^{\mathrm{T}} \tag{1}$$

## 2.1 Equivalent stiffness and damping models of a loosened pedestal

When one or a few bolts become loosened and vibration increases seriously, the pedestal and the base may be separated partially. Assuming that the right pedestal is loosened in a vertical direction, $y_{\mathrm{p}}$ is pedestal displacement and $\delta_1$ is the looseness clearance, as is shown in Fig. 2. The right side of Fig. 2 displays the simplified spring-mass-damping model of the loosened pedestal, where $k_y^r, c_y^r$ are stiffness and damping of the right bearing, $m_p^r$ is right pedestal mass and $k_b^r, c_b^r$ are equivalent stiffness and damping of the pedestal, respectively. When $y_{\mathrm{p}} = 0$, the pedestal is in contact with the base. $y_{\mathrm{p}} < 0$ means that the pedestal and the base are in compression state and the impact is considered elastic, here $k_b^r$ is the base stiffness $k_b$. Non-loosened bolts will be in a state of elastic deformation due to the pulling force and $k_b^r$ is the stiffness of non-loosened bolts $k_{b1}$ when $0 \le y_{\mathrm{p}} \le \delta_1$. $y_{\mathrm{p}} > \delta_1$ describes the extension of the loosened bolts and non-loosened bolts, the deformation of the bolts are assumed as elastic, here $k_b^r$ is $k_{b1} + k_{b2} - k_{b2}\dfrac{\delta_1}{y_{\mathrm{p}}}$ ($k_{b2}$ is the stiffness of loosened bolts). From the above analysis, it is clear that $k_b^r$ is a piecewise function related to $y_{\mathrm{p}}$ and its expression [3] can be written as follows

$$k_b^r = \begin{cases} k_b & y_{\mathrm{p}} < 0 \\ k_{b1} & 0 \le y_{\mathrm{p}} \le \delta_1 \\ k_{b1} + k_{b2} - k_{b2}\dfrac{\delta_1}{y_{\mathrm{p}}} & y_{\mathrm{p}} > \delta_1 \end{cases}. \tag{2}$$

Assuming that base stiffness is approximately equal to tensile stiffness of the bolts, namely, $k_b \approx k_{b1} + k_{b_2} - k_{b2}\dfrac{\delta_1}{y_{\mathrm{p}}}$, then Eq. (2) can be simplified as

$$k_b^r \approx \begin{cases} k_{b1}, & 0 \le y_{\mathrm{p}} < \delta_1 \\ k_b, & \text{others} \end{cases}. \tag{3}$$

The equivalent damping of the right pedestal $c_b^r$ is similar to $k_b^r$, and its expression is as follows

$$c_b^r \approx \begin{cases} c_{b1}, & 0 \le y_{\mathrm{p}} < \delta_1 \\ c_b, & \text{others} \end{cases}. \tag{4}$$


ISSN 2572-4975 (Print), 2572-4991 (Online)

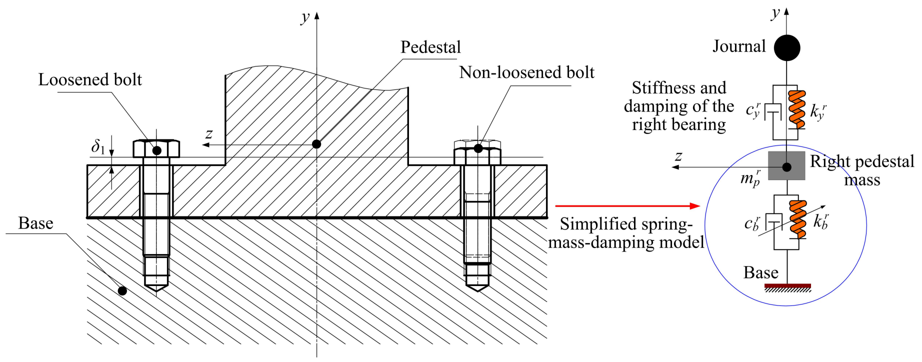


**Fig. 2.** Bolt looseness schematic diagram

## 2.2 The rotor-stator fixed-point rubbing model

The rotor-stator rubbing can be regarded as a contact problem with friction and an initial gap. It is assumed that the rotor-stator rubbing appears between two fixed points in the rotor and a stator (fixed limiting stop), as is shown in Fig. 3. In the figure, o is the whirl center of the rotor, or the geometric center of the rotor and ω the rotating speed. In order to simplify the modeling process and shorten the FE simulation time, the contact form is treated as a point-point contact. The master body is set as the rotor and the slave one is the stator. It is assumed that the cross-section of the disc remains in the yoz plane and contact only occurs in a positive y-axis direction. Point c in the disc and point d in the stator are selected as a contact pair shown in Fig. 3, so the gap function g is equal to the distance.

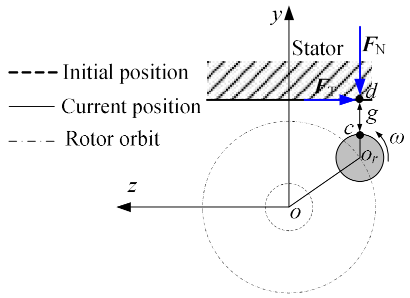


**Fig. 3.** fixed-point rubbing model scheme

Thermal effects and friction torque are ignored during the rubbing process, and only normal and tangential rubbing forces ($\boldsymbol{F}_{\mathrm{N}}$ and $\boldsymbol{F}_{\mathrm{T}}$) are considered. Generally, normal contact force $\boldsymbol{F}_{\mathrm{N}}$ can be expressed as the product of a non-negative scalar $F_{\mathrm{N}}$ and the unit outward vector **n**. Based on contact dynamic theory [25-27], two contact points *c* and *d* must satisfy the following Kuhn-Tucker impenetrability conditions:

$$\begin{cases} F_{\mathrm{N}} \geq 0 \\ g \leq 0 \\ F_{\mathrm{N}} \cdot g = 0 \end{cases} .. \tag{5}$$

Eq. (5) implies vanishing of $F_{\mathrm{N}}$ in the case of separation or the vanishing of $g$ in the case of contact.

Friction is often an essential consideration for a contact problem. Although various friction schemes have been proposed, the Coulomb friction law is still one of the most widely accepted models to describe the friction phenomenon. The Kuhn-Tucker conditions for Coulomb friction are as follows:

$$\phi = \left\| \boldsymbol{F}_{\mathrm{T}} \right\| - \mu_{\mathrm{f}} F_{\mathrm{N}} \leq 0 ,. \tag{6}$$

$$\dot{\boldsymbol{g}}_{\mathrm{T}} = \xi \frac{\partial}{\partial \boldsymbol{F}_{\mathrm{T}}} \phi , \tag{7}$$

$$\begin{cases} \xi \geq 0 \\ \xi\phi = 0 \end{cases} . \tag{8}$$

where $\| \ \|$ denotes L2 norm, $\mu_{\mathrm{f}}$ is the friction coefficient and $\boldsymbol{g}_{\mathrm{T}}$ is the tangential gap. According to Eqs. (7) and (8), it is clear that perfect stick contact occurs when $\phi < 0$ and slip contact occurs when $\phi = 0$.

The augmented Lagrangian method is adopted to deal with contact constraint conditions. The augmented Lagrangian statement of the friction law is expressed as follows:

$$\begin{cases} F_{\mathrm{N}} = \left\langle \lambda_{\mathrm{N}} + \varepsilon_{\mathrm{N}} g \right\rangle \\ \phi = \left\| \boldsymbol{F}_{T} \right\| - \mu_{\mathrm{f}} F_{\mathrm{N}} \leq 0 \\ \dot{\boldsymbol{g}}_{\mathrm{T}} - \xi \frac{\partial}{\partial \boldsymbol{F}_{\mathrm{T}}} \phi = \frac{1}{\varepsilon_{\mathrm{T}}} (\dot{\boldsymbol{F}}_{\mathrm{T}} - \dot{\boldsymbol{\lambda}}_{\mathrm{T}}) \\ \xi \geq 0 \\ \xi\phi = 0 \end{cases} ,. \tag{9}$$

where $\varepsilon_{\mathrm{N}} > 0$ is the penalty parameter in the normal direction (normal contact stiffness) and $\lambda_{\mathrm{N}}$ is the Lagrange multiplier. The tangential traction $\boldsymbol{F}_{\mathrm{T}}$ contains the penalty part and the Lagrange multiplier part wherein $\boldsymbol{\lambda}_{\mathrm{T}}$ denotes the tangential Lagrange multiplier of $\boldsymbol{F}_{\mathrm{T}}$, and $\varepsilon_{\mathrm{T}}$ is the tangent penalty parameter. Assuming that system response at $t = T_n$ is known, the complete augmentation equations for the contact tractions are listed as follows:

$$\begin{cases} F_{\mathrm{N}_{n+1}} = \left\langle \lambda_{\mathrm{N}_{n+1}} + \varepsilon_{\mathrm{N}} g_{n+1} \right\rangle \\ \boldsymbol{F}_{\mathrm{T}_{n+1}} = \boldsymbol{F}_{\mathrm{T}_n} + \Delta\boldsymbol{\lambda}_{\mathrm{T}} + \varepsilon_{\mathrm{T}} (\Delta\boldsymbol{g}_{\mathrm{T}} - \Delta\xi \boldsymbol{F}^{\mathrm{trial}}_{\mathrm{T}_{n+1}} / \left\| \boldsymbol{F}^{\mathrm{trial}}_{\mathrm{T}_{n+1}} \right\|) \end{cases} , \tag{10}$$


ISSN 2572-4975 (Print), 2572-4991 (Online)

where

$$\begin{cases} \Delta\boldsymbol{\lambda}_{\mathrm{T}} = \boldsymbol{\lambda}_{\mathrm{T}_{n+1}} - \boldsymbol{\lambda}_{\mathrm{T}_{n+1}} \\ \Delta\boldsymbol{g}_{\mathrm{T}} = \boldsymbol{g}_{\mathrm{T}_{n+1}} - \boldsymbol{g}_{\mathrm{T}_{n}} \\ \boldsymbol{F}_{\mathrm{T}_{n+1}}^{\mathrm{trial}} = \boldsymbol{F}_{T_n} + \Delta\boldsymbol{\lambda}_{\mathrm{T}} + \varepsilon_{\mathrm{T}}\Delta\boldsymbol{g}_{\mathrm{T}_{n+1}} \\ \Delta\xi = \begin{cases} 0, & \phi_{n+1}^{\mathrm{trial}} \le 0 \\ \dfrac{\phi_{n+1}^{\mathrm{trial}}}{\varepsilon_{\mathrm{T}}}, & \phi_{n+1}^{\mathrm{trial}} > 0 \end{cases} \end{cases}, \tag{11}$$

### 2.3 The finite element model of a rubbing rotor system in the presence of the pedestal looseness

Considering the effects of the pedestal looseness, the fixed-point rubbing and the external forces on the system vibration, the equation of motion of the system can be written as follows:

$$\begin{bmatrix} \boldsymbol{M} & \boldsymbol{0} \\ \boldsymbol{0} & \boldsymbol{0} \end{bmatrix} \begin{bmatrix} \ddot{\boldsymbol{u}} \\ \boldsymbol{0} \end{bmatrix} + \begin{bmatrix} \boldsymbol{G}+\boldsymbol{C} & \boldsymbol{0} \\ \boldsymbol{0} & \boldsymbol{0} \end{bmatrix} \begin{bmatrix} \dot{\boldsymbol{u}} \\ \boldsymbol{0} \end{bmatrix} + \begin{bmatrix} \boldsymbol{K}+\varepsilon_{\mathrm{N}}\boldsymbol{B}^{\mathrm{T}}\boldsymbol{B} & \boldsymbol{B}^{\mathrm{T}} \\ \boldsymbol{B} & \boldsymbol{0} \end{bmatrix} \begin{bmatrix} \boldsymbol{u} \\ \boldsymbol{\lambda} \end{bmatrix} = \begin{bmatrix} \boldsymbol{F}_u - \varepsilon_{\mathrm{N}}\boldsymbol{B}^{\mathrm{T}}\boldsymbol{g}_0 \\ -\boldsymbol{g}_0 \end{bmatrix} \tag{12}$$

where $\boldsymbol{M}$, $\boldsymbol{G}$, $\boldsymbol{C}$, $\boldsymbol{K}$ and $\boldsymbol{u}$ respectively denote the mass matrix, the gyroscopic matrix, the damping matrix (including the bearing damping, the equivalent damping of the loosened pedestal and viscous damping) and the stiffness matrix (including the rotor stiffness, the bearing stiffness and the equivalent stiffness of the loosened pedestal) matrixes and the displacement vector of the global system respectively $\boldsymbol{\lambda}$ is a vector about the Lagrange multiplier, $\boldsymbol{B}$ is the contact constraint matrix in the normal and tangential directions, $\boldsymbol{g}_0$ is the initial normal gap vector, $\boldsymbol{F}_u$ is the external load vector. In this paper, Rayleigh damping form is applied to determine the viscous part ($\boldsymbol{C}_s$) of the total damping matrix ($\boldsymbol{C}$) and it can be obtained by the following formula [28]:

$$\boldsymbol{C}_s = \alpha\boldsymbol{M} + \beta\boldsymbol{K} \,,. \tag{13}$$

where

$$\alpha = \frac{\pi(\omega_{\mathrm{n}2}\xi_1 - \omega_{\mathrm{n}1}\xi_2)\omega_{\mathrm{n}1}\omega_{\mathrm{n}2}}{15(\omega_{\mathrm{n}2}^2 - \omega_{\mathrm{n}1}^2)}, \beta = \frac{60(\omega_{\mathrm{n}2}\xi_2 - \omega_{\mathrm{n}1}\xi_1)}{\pi(\omega_{\mathrm{n}2}^2 - \omega_{\mathrm{n}1}^2)} \tag{14}$$

herein $\omega_{\mathrm{n}1}$ and $\omega_{\mathrm{n}2}$ respectively stand for the first and second critical speeds (r/min) of the rotor system, $\xi_1$ and $\xi_2$ are corresponding modal damping ratios, respectively. The FE model of a rubbing rotor system with one pedestal looseness is shown in Fig. 4. In the figure, node 19 denotes the position of disc 2, rub-impact occurs at node 23 and the right bearing is located at node 26. Nonlinear differential equations considering both rotor-stator rubbing and pedestal looseness, Eq. (12), is solved by using Newmark-$\beta$ method combined with Newton-Raphson iteration.

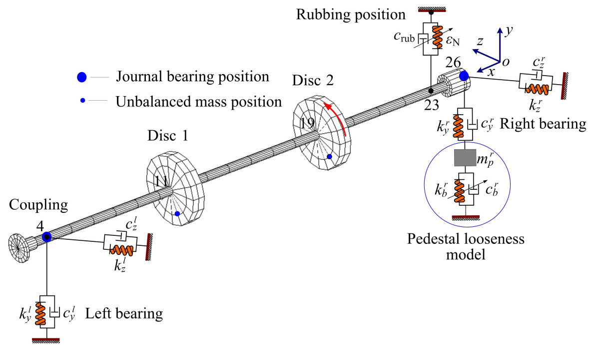


**Fig. 4.** The FE model of rotor system with the pedestal looseness coupled rub-impact fault

## 3 Fault characteristic analysis of the rotor system with rubbing fault in the presence of the pedestal looseness

The geometric dimensions of the rotor system can be found in literature [29], other model parameters of the rotor system with rubbing in the presence of pedestal looseness are listed in Table 1. The first and second critical speeds ($\omega_{n1}$ and $\omega_{n2}$) of the rotor system without faults are 1680 r/min and 6450 r/min based on the parameters in Table 1. The influences of the rotating speed and the stiffness of non-loosened bolts on the dynamics of the rotor system with rubbing fault in the presence of pedestal looseness will be discussed in the following sections and descriptions about the figures and their corresponding model parameters are shown in Table 2.

**Table 1.** Model parameters of the rotor system

| | | | | |
|---|---|---|---|---|
| Material parameters | Elastic modulus $E$ (GPa) | Poisson's ratio $\upsilon$ | Density $\rho$ (kg/m$^3$) | The first and second modal damping ratios ($\xi_1 = \xi_2$) |
| | 207 | 0.3 | 7850 | 0.04 |
| Bearing parameters | Horizontal stiffness $k_z^l = k_z^r$ (MN/m) | Vertical stiffness $k_y^l = k_y^r$ (MN/m) | Horizontal damping $c_z^l = c_z^r$ (kN·s/m) | Vertical damping $c_y^l = c_y^r$ (kN·s/m) |
| | 200 | 500 | 2 | 2 |
| Pedestal parameters without loosenss | The base stiffness $k_b$ (MN/m) | Pedestal damping $c_b$ (kN·s/m) | Right Pedestal mass $m_p^r$ (kg) | ---- |
| | 200 | 0.2 | 1.256 | |
| Residual unbalance | Eccentricity of unbalance mass of disc 1 $mr$ (g·m) | Eccentric phase angle of unbalance mass at disc 1 (°) | Eccentricity of unbalance mass of disc 2 $mr$ (kg·m) | Eccentric phase angle of unbalance mass at disc 2 (°) |
| | 0.156 | 0 | 0.156 | 0 |


ISSN 2572-4975 (Print), 2572-4991 (Online)

| Parameters about rubbing | Normal contact stiffness $\varepsilon_N$ (MN/m) | Contact damping $c_{rub}$ (N·s/m) | the friction coefficient $\mu_f$ | ---- |
|---|---|---|---|---|
| | 80 | 0 | 0.3 | |

Note: superscripts $l$ and $r$ denote left and right bearings respectively.

**Table 2.** Descriptions about the figures and their corresponding model parameters

| Changing parameters | Fault types | $\delta_1$(m m) | $\kappa$=log($k_{b1}$/2) | $c_{b1}$(N·s/m) | $g_0$ (μm) | $\gamma=\omega/\omega_{n1}$ | Figures concerned |
|---|---|---|---|---|---|---|---|
| The influence of the rotating speeds in Section 3.1 | Rubbing | ---- | ---- | ---- | 80 | 0.5,1,1.5,2,2.5,3, 3.5,4,4.5,5,5.5,6 | Figs. 5(a),6 |
| | Pedestal looseness | A value at $\delta_1>y_p$ | 4 | 125 | ---- | 0.5,1,1.5,2,2.5,3, 3.5,4,4.5,5,5.5,6 | Figs. 7(a),8 |
| | Fault coupling | A value at $\delta_1>y_p$ | 4 | 125 | 80 | 0.5,1,1.5,2,2.5,3, 3.5,4,4.5,5,5.5,6 | Figs.5(b),6,7(b),8 |
| $k_{b1}$ when $y_p\le\delta_1$ in Section 3.2 | Rubbing | ---- | ---- | ---- | 50 | 1 | Fig. 11 |
| | Pedestal looseness | A value at $\delta_1>y_p$ | 0,1,2,3,4,5,6,7,8 | Table 3 | ---- | 1 | Figs 9(a),10(a) |
| | Fault coupling | A value at $\delta_1>y_p$ | 0,1,2,3,4,5,6,7,8 | Table 3 | 50 | 1 | Figs 9(b),10(b),11 |
| $k_{b1}$ when $y_p>\delta_1$ in section 3.3 | Rubbing | ---- | ---- | ---- | 50 | 1 | Fig. 15 |
| | Pedestal looseness | 1 | 0,1,2,3,4 | Table 3 | ---- | 1 | Fig. 12(a),13,14(a) |
| | Fault coupling | 0.25 | 0,1,2,3,4 | Table 3 | 50 | 1 | Figs. 12(b),13,14(b),15 |

Note: Fault coupling denotes rubbing in the presence of pedestal looseness; the unit of $k_{b1}$ is N/m

### 3.1 The influence of rotating speeds when $y_p \le \delta_1$

According to reference [5], the vibration of the rotor system with pedestal looseness is violent and its fault features are more complicated when $y_p \le \delta_1$. So in this section, the influence of rotating speed is discussed only under the condition of $y_p \le \delta_1$. This condition indicates that the stiffness changes only when the pedestal contacts the base. Spectrum cascades of the rotor system (node 23) are shown in Fig. 5 under single rubbing and fault coupling between the rubbing and the pedestal looseness. For the spectrum cascade, the right-hand abscissa is ratio of the rotating speed to the first critical speed ($\gamma=\omega/\omega_{n1}$), the left-hand abscissa is frequency (Hz) and the ordinate is the dimensionless amplitude in $y$ direction. The dimensionless amplitude is determined by the original amplitude divided by the biggest amplitude among all the frequency components in Fig. 5. In this paper, the amplitude of 1×/2 at $\gamma$=2.5 in Fig. 5(b) is the biggest and selected as denominator to obtain the dimensionless amplitude.

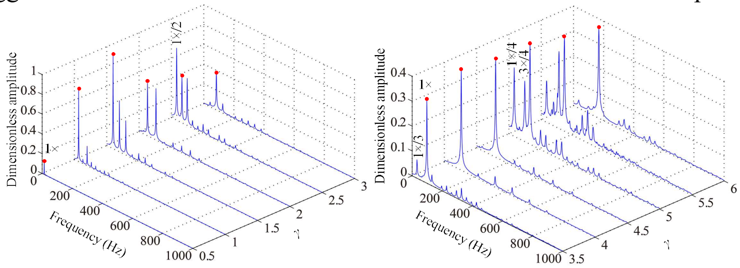


(a) Spectrum cascades of node 23 under the single rubbing condition

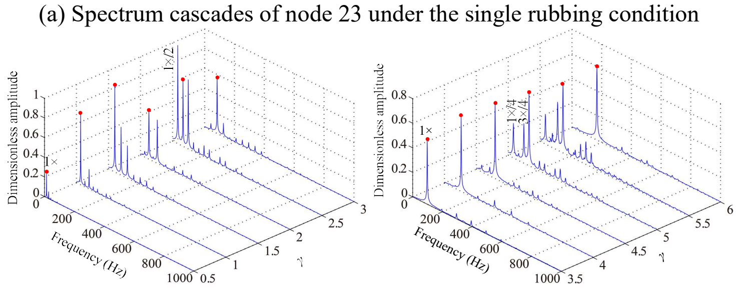


(b) Spectrum cascades of node 23 under the rubbing condition in the presence of pedestal looseness

**Fig. 5.** Spectrum cascades of node 23 under two fault conditions

For the single rubbing fault, spectrum cascades of node 23 are shown in Fig. 5(a). The figure displays that no rubbing appears at $\gamma$=0.5 in the rotor system. The multiple harmonic components ($n$×, $n$=1, 2…) can be observed at $\gamma$=1,1.5,2. The 1/2 fractional harmonic components such as 1×/2, 3×/2, etc. appear at $\gamma$=2.5,3, so the rotor motion is period-two (P2). Particularly, the amplitude of 1×/2 is larger than that of 1× at $\gamma$=2.5. The 1/3 fractional harmonic components such as 1×/3, 4×/3, etc. exist, which means that system motion is period-three (P3) at $\gamma$=3.5. Multiple harmonic components with small amplitudes appear again at $\gamma$=4, here the rotor has a period-one motion (P1). Combination frequency components related to 1× appear, and the system motion is quasi-period at $\gamma$=4.5. There are 1/4 fractional harmonic components such as 1×/4, 3×/4, etc in spectrum cascades at $\gamma$=5, which shows the system motion is period-four (P4). However, quasi-period motions appear again at $\gamma$=5.5,6. The amplitudes of low combination frequency components are all larger at $\gamma$=5.5.

For the rubbing fault in the presence of pedestal looseness, the responses of node 23 (the rubbing position) possess different dynamic features compared with those under the single rubbing condition. At $\gamma$=0.5, multiple harmonic components ($n$×, $n$=1, 2…) exist in the spectrum cascade, which indicates that the rubbing occurs. The system motion in both cases is P1 at $\gamma$=1,1.5. The system is P2 at $\gamma$=2,2.5,3, however the system is P1 at $\gamma$=2 for the single rubbing case. For the rubbing fault in the presence of pedestal looseness, the system motion is P1 at $\gamma = 4$ but the system motion is P3 at $\gamma$=3.5 and quasi-periodic at $\gamma = 4$ for the single rub-impact fault. The system motion is quasi-periodic at $\gamma$=4.5,5,5.5,6 for both cases.

Some typical vibration responses at node 23 are shown in Fig. 6 under single rubbing and rubbing in the presence of pedestal looseness conditions. From left to right, the figure shows time domain waveform, rotor orbit, normal contact force and contact state, respectively. In the figures, the red lines and points denote single rubbing and the blue lines and dot lines denote rubbing in the presence of pedestal looseness. The contact state is presented by three numbers; "1" denotes non-contact of the rotor and the stator, "2" sliding contact and "3" sticking contact (no sliding).

The vibration responses of the system at $\gamma$=2 are shown in Fig. 6(a). It can be seen from the figure that the time waveform shows the existence of two periods, rotor orbit indicates two circles and the contact state changes from sliding contact state to alternate sliding and sticking contact states under the condition of rubbing with pedestal looseness. These vibration characteristics are different from those of the single rubbing indicating the effect of the fault coupling. System motion for the fault coupling and the single fault conditions shows a greater difference at $\gamma$=3.5, as is shown in Fig. 6(b). From the figure, it is clear that the collision rebound is serious, collision times less and contact state shows alternate sliding and sticking contacts for single rubbing compared with the fault coupling. The results also imply that the sticking contact appears under the condition of larger normal rubbing force. For rubbing and rubbing with pedestal looseness conditions, when $\gamma$=4, the waveforms and rotor orbits are all similar, while the normal contact forces and states show a little difference. For the same system motion under both fault conditions, the vibration responses are much the same at $\gamma$=5.

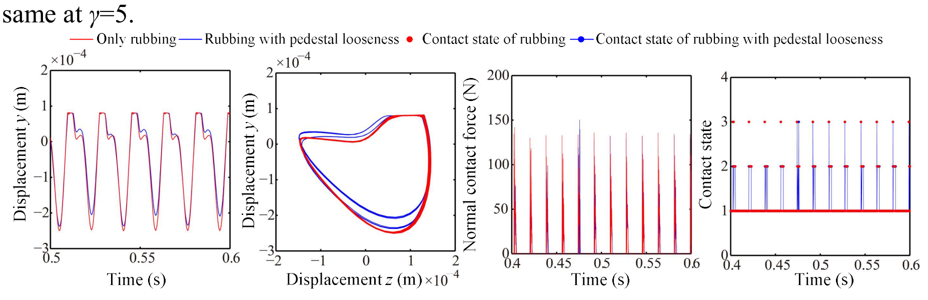


(a) $\gamma$=2

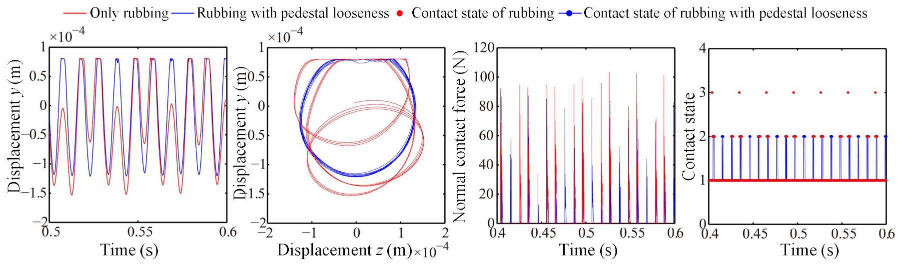


(b) $\gamma$=3.5

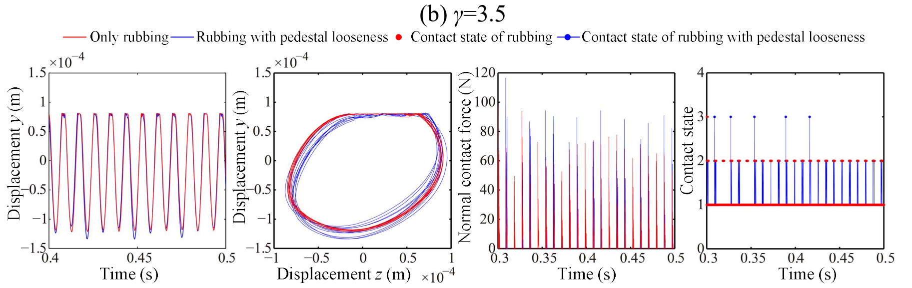


(c) $\gamma$=4

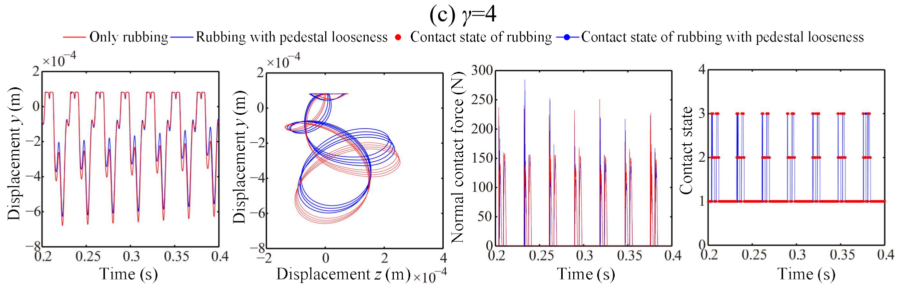


(d) $\gamma$=5

**Fig. 6.** Vibration response of the rotor system under single rubbing and rubbing in the presence of pedestal looseness conditions (node 23)

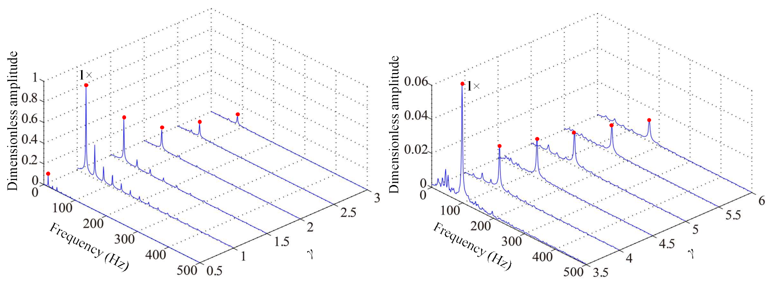


(a) Spectrum cascades of node 26 under the single pedestal looseness condition


ISSN 2572-4975 (Print), 2572-4991 (Online)

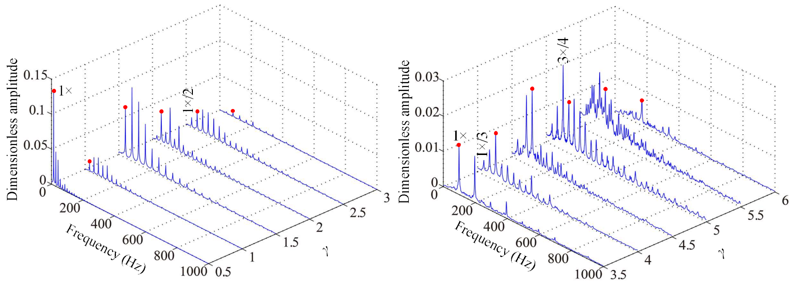


(b) Spectrum cascades of node 26 under the rubbing condition in the presence of pedestal looseness

**Fig. 7.** Spectrum cascades of node 26 under two fault conditions

Spectrum cascades of the rotor system (node 26 at pedestal position) are shown in Fig. 7 under single pedestal looseness and fault coupling of rubbing and pedestal looseness conditions. It can be observed clearly from Fig. 7(a) that when only pedestal looseness fault occurs, system response shows multiple harmonic components ($n$×, $n$=1, 2, 3…) at $\gamma$=0.5,1,1.5,2 indicating that the system motion is P1; 1×/$\gamma$ factional harmonic components can be observed at $\gamma$=3,4,5, which shows the system motion is period-$\gamma$ ; at $\gamma$=2.5,3.5,4.5,5.5, the system motion is quasi-periodic because the frequency spectrum shows the combination frequency components of the rotating frequency and the first natural frequency $f_{r1}$ ($f_{r1}=\omega_{n1}/60$).

The responses of node 26 under the fault coupling condition are shown in Fig. 7(b). $n$×( $n$=1, 2…) appears for both cases at $\gamma$=0.5,1,1.5, however, the amplitudes of 2× and 3× are greater than that of 1× for the fault coupling condition at $\gamma$=1,1.5. System motion is only P2 at $\gamma$=2,2.5,3, while P1, quasi-periodic and P3 respectively for the single fault. At $\gamma$=3.5, $n$×($n$=1, 2…) and combination frequency components with complicated low frequency exist for both cases. System motion is P3 for the fault coupling case, but P4 for the single pedestal at $\gamma$=4. System motions are both quasi-periodic at $\gamma$=4.5. However, only low combination frequency components appear for the single pedestal looseness fault while many high combination frequency components exist for the fault coupling case. System motions are P4 and P5 at $\gamma$=5 for the fault coupling and single fault cases respectively. For the fault coupling case, system motions at $\gamma$=5.5,6 are both quasi-periodic and the amplitudes of many combination frequency components are greater than that of 1×, however, they are quasi-periodic and P6 respectively for the single pedestal looseness case.

The system responses with some typical motion patterns are shown in Fig. 8 under single pedestal looseness and rubbing in the presence of pedestal looseness conditions. From top to bottom, the figures in the upper line and lower line shows the time domain waveform and the rotor orbit at $\gamma$=1,2.5,3.5,5.5, respectively. From the variation of the waveform and the rotor orbit, it can be seen that pedestal looseness has a greater influence on local vibration of looseness end, namely vibration is more violent. Time domain waveform of node 26 is asymmetric in looseness direction and the vibration in positive $y$ direction is obviously greater than that in negative $y$ direction. This is because the equivalent pedestal stiffness decrease causes constraint decline of rotor motion when the pedestal separates from the base; while the looseness disappears when the pedestal contacts the base. The smaller vibration amplitude of node 26 in $y$ negative direction can be considered as a typical symptom of pedestal looseness. The contact time can be determined by the clipping length and contact times by the trough numbers of the waveform whose displacement is close to zero. Based on the above-mentioned features, it can be concluded that the contact time between the pedestal and the base is the longest at $\gamma = 1$ , the contact bounce becomes aggravated and collision times decrease with the increase of the rotating speed. For the fault coupling condition, the vibration of node 26 is limited due to the rubbing, and the vibration amplitude sharply decreases at $\gamma$=1,2.5,3.5.

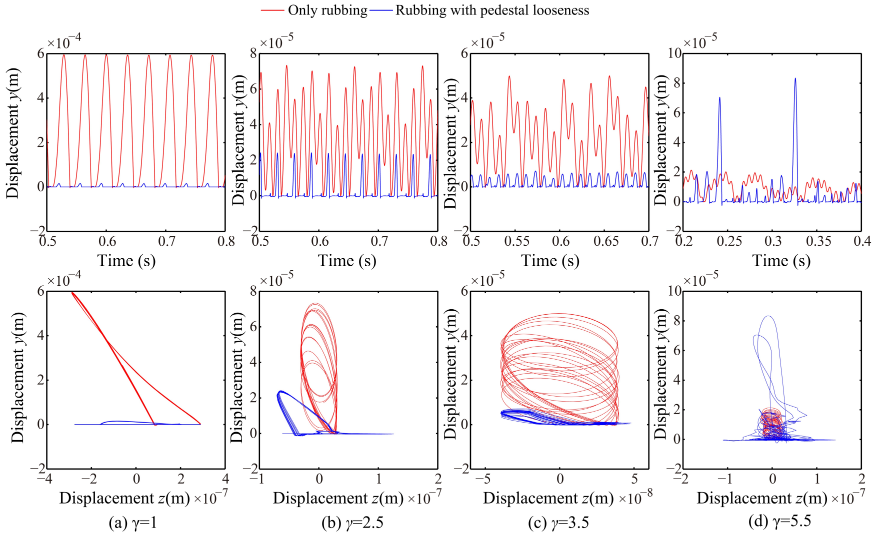


**Fig. 8.** Vibration response of the rotor system under single pedestal looseness and rubbing in the presence of pedestal looseness conditions (node 26)

### 3.2 The influence of the stiffness of non-loosened bolts when $y_p \le \delta_1$

In this section, it is assumed that pedestal displacement is less than or equal to looseness clearance ($y_p \le \delta_1$), the rotating speed is equal to the first critical speed 1680 r/min ($\omega=\omega_{n1}$), $g_0$ is adjusted as $g_0$=50 μm to study the rubbing under pedestal looseness condition and the pedestal equivalent damping changes with different stiffnesses of non-loosened bolts, as is shown in Table 3. Other parameters are the same as those in Section 3.1.

**Table 3.** Stiffness and damping parameters of non-loosened bolts-

| Stiffness of non-loosened bolts $k_{b1}$/(N/m) | $\kappa$=log($k_{b1}$/2) | Damping of non-loosened bolts $c_{b1}$/(N·s/m) |
|---|---|---|
| $2\times10^8$ | 8 | 2 000 |
| $2\times10^7$ | 7 | 1 000 |
| $2\times10^6$ | 6 | 500 |

| | | |
|---|---|---|
| $2\times10^5$ | 5 | 250 |
| $2\times10^4$ | 4 | 125 |
| $2\times10^3$ | 3 | 62.5 |
| $2\times10^2$ | 2 | 31.25 |
| $2\times10^1$ | 1 | 15.63 |
| 2 | 0 | 7.81 |

System vibration responses of node 23 under single pedestal looseness and rubbing in the presence of pedestal looseness conditions are shown in Fig. 9. For the spectrum cascade, the right-hand abscissa is the pedestal equivalent stiffness ($\kappa$=log($k_{b1}$/2)); the left-hand abscissa and the ordinate are the same as those in Fig. 7 . For the single pedestal looseness, some low frequency components appear, such as 1×/2 at $\kappa$=3, as is shown in Fig. 9(a). For the fault coupling condition, it can be observed that frequency components are mainly multiple components ($n$×, $n$=1, 2…) at different stiffnesses of non-loosened bolts, the amplitude of 4× is always second to that of 1× because 4× is close to the second natural frequency, as is shown in Fig. 9(b).

System vibration responses of node 26 under single pedestal looseness and rubbing in the presence of pedestal looseness conditions are shown in Fig. 10. For the single looseness fault case, high-order super-harmonics only appear at the larger stiffness of non-loosened bolts and lower frequency components appear with decrease of the stiffness of non-loosened bolts, as is shown in Fig. 10(a). For the fault coupling condition, diverse multiple frequency components can be observed, which are similar to those of node 23. It is clear that the features of the rubbing appear while the features of the pedestal disappear, namely, the rubbing is dominant under the fault coupling condition due to its severity and the range of its potential influence.

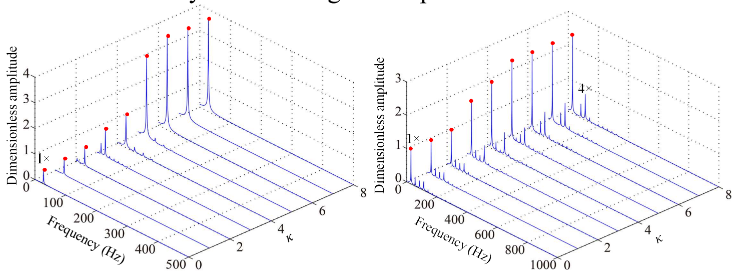


(a) The single pedestal looseness (b) Rubbing in the presence of pedestal looseness $y_p \le \delta_1$

**Fig. 9.** Spectrum cascades of node 23 under two conditions

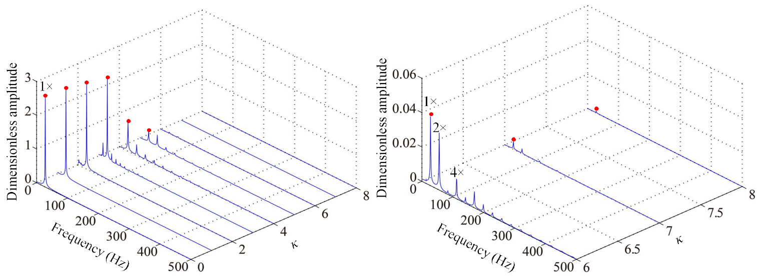


(a) Single pedestal looseness

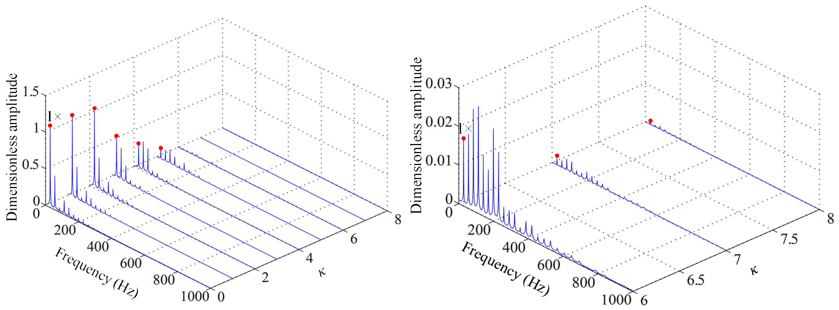


(b) Rubbing in the presence of pedestal looseness

**Fig. 10.** Spectrum cascades of node 26 under two conditions

The vibration responses of node 23 are shown in Fig. 11 at $\kappa$=2,4. The red lines (points) show the responses under single rubbing fault case and the blue lines (dot line) show the responses under fault coupling case. The vibration under the single rubbing condition is much more violent than that under the rubbing with pedestal looseness condition at $\kappa$=2 while the vibration intensity under both case are slightly different at $\kappa$=4. These results also imply that the pedestal looseness can reduce the rubbing intensity under some stiffness of non-loosened bolts conditions, such as $\kappa$=2.

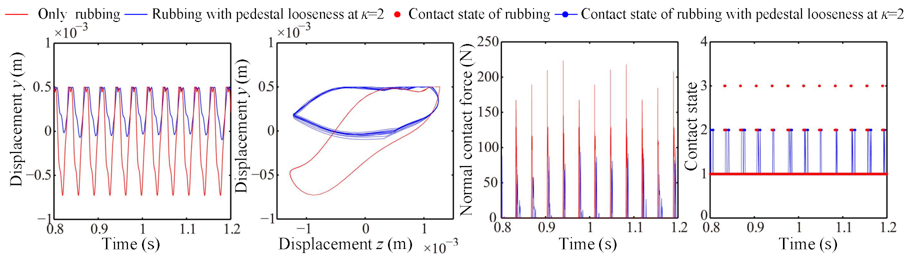


(a) $\kappa$=2

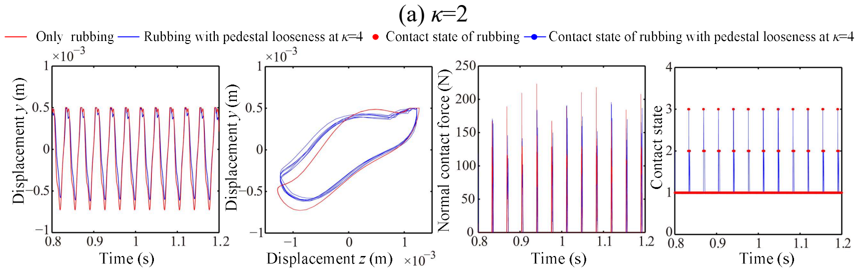


(b) $\kappa$=4

**Fig. 11.** Vibration responses under different stiffnesses of non-loosened bolts (node 23)

### 3.3 The influence of the stiffness of non-loosened bolts when $y_b>\delta_1$

If the vibration displacement of the pedestal $y_b$ is greater than the looseness clearance $\delta_1$ under the rotor-stator rubbing condition, namely $y_b>\delta_1$, here the looseness condition is similar to the constraint of a double face. The rotor-stator gap $g_0$, looseness clearance $\delta_1$ and other model parameters are shown in Table 2. The vibration responses of node 23 are shown in Fig. 12 under the single pedestal looseness and fault coupling of rubbing and pedestal looseness conditions.

For the single pedestal looseness, loosened bolts limit the pedestal upward displacement and the bilateral collision appears when $y_b>\delta_1$ ($\delta_1$=1mm) at $\kappa$=0,1,2,3, as is shown in Fig. 12(a). The frequency components of the system include 1×, the second natural frequency $f_{r2}$ ($f_{r2}=\omega_{n2}/60$). and their combination frequencies, so the system motion is quasi-periodic. The system motion is P1 when the pedestal displacement is less than the looseness clearance at $\kappa$=4. The vibration waveforms and rotor orbits of node 23 at $\kappa$=2,4 are shown in Fig. 13. From the figure, it is clear that the waveform caused by the bilateral collision ($y_b>\delta_1$) at $\kappa$=2 is irregular compared with that caused by the unilateral collision at $\kappa$=4 where $y_b<\delta_1$.

For the rubbing in the presence of pedestal looseness, the system responses show multiple harmonic components ($n$×, $n$=1, 2…) under different $\kappa$. For the response at node 23, the amplitude of 4× is second to that of 1× because 4× is close to the second natural frequency. However, for the response of node 26, high frequency components are more dominant because their amplitudes are very large with respect to that of 1×; the amplitude of 3× is largest, that of 2× is second and both of them are greater than that of 1×. The system vibration response under bilateral constraint condition is close to that under single constraint condition with larger $\kappa$.

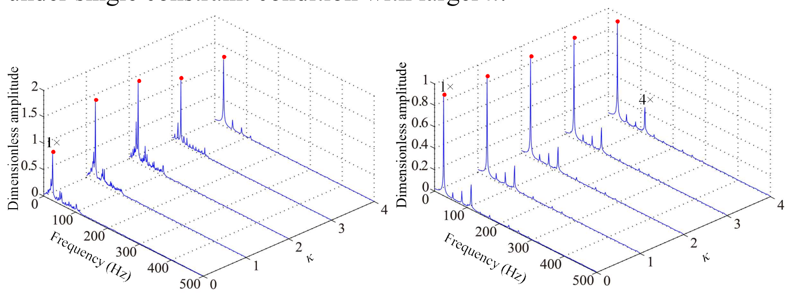


(a) The single pedestal looseness (b) Rubbing in the presence of pedestal looseness when $y_b \geq \delta_1$

**Fig. 12.** Spectrum cascades of node 23 under two conditions

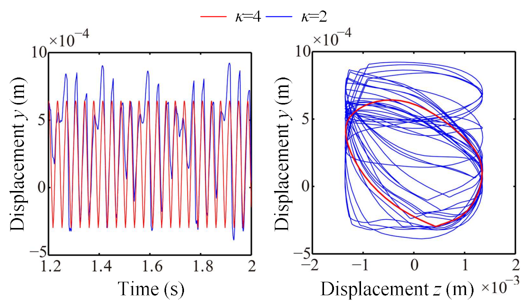


**Fig. 13.** Vibration responses of node 23 at $\kappa$=2,4

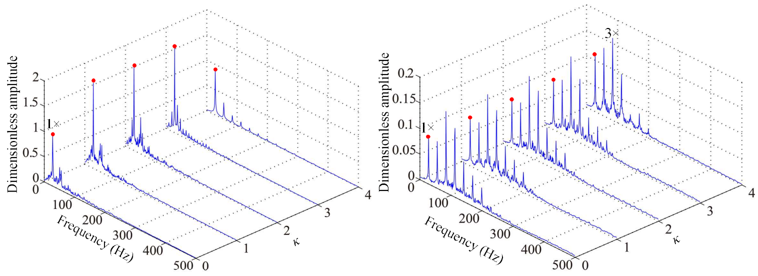


(a) The single pedestal looseness (b) Rubbing in the presence of pedestal looseness when $y_b \geq \delta_1$

**Fig. 14.** Spectrum cascades of node 26 under two conditions

Fig. 15 shows vibration responses of node 23 under single rubbing and fault coupling of rubbing and pedestal looseness conditions. From the figure, it can be seen that the waveform, rotor orbit, contact force and contact state are similar, which implies that the bilateral constraint caused by the small looseness clearance can restrain pedestal vibration to some extent.

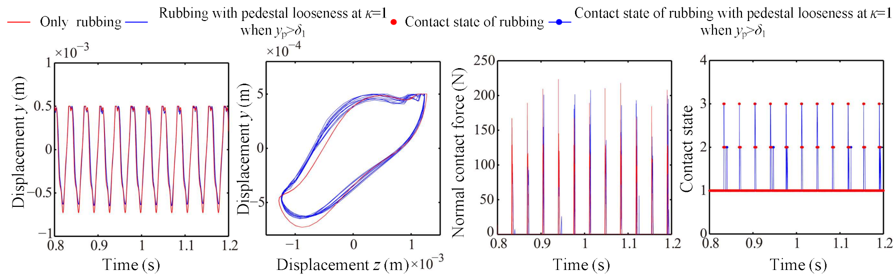


**Fig. 15.** Vibration responses of node 23 under single rubbing and fault coupling of rubbing and pedestal looseness conditions

## 4 Conclusions

In this study, a finite element model of a rubbing rotor system in the presence of pedestal looseness is established; system fault characteristics are investigated based on contact dynamics considering the effects of the rotating speeds and the stiffness of non-loosened bolts. The results show that the rubbing fault plays a dominant role in the rubbing rotor system in the presence of pedestal looseness and the pedestal looseness only affects the local scope of loosened pedestal. The system motion is from P1 through P2, P1 and P3 successively to quasi-periodic motion with the increase of rotating speeds. The change of the motion patterns is different from that under the single rubbing conditions when the rotating speeds are 2,3.5 and 4 times of the first critical speed, and the system motion is the same at other rotating speeds under two fault conditions.

With the decrease of the stiffness of the non-loosened bolts, the vibration displacement decreases at the rub-impact location; however, vibration displacement increases at the pedestal looseness location when the pedestal displacement is less than the looseness clearance. The rubbing intensity can be weakened under some stiffnesses of the non-loosened bolts. Multiple harmonic components, especially 4× with larger amplitude can be viewed as typical fault features. When the stiffness of the non-loosened bolts changes, the vibration characteristics of the system are almost the same and the higher harmonics with continuous spectra at looseness location can be observed when the pedestal displacement is greater than the looseness clearance condition. Under this condition, the fault coupling features are similar to those of the single rubbing.

## Acknowledgement

This project is supported by the Joint Funds of the National Natural Science Foundation and the Civil Aviation Administration of China (Grant no. U1433109), the Fundamental Research Funds for the Central Universities (Grant nos. N150305001 and N140301001) and State Key Laboratory for Strength and Vibration of Mechanical Structures (Grant no. SV2015-KF-08) for providing financial support for this work.

## References

1. A. Muszynska, Rotordynamics, CRC Taylor & Francis Group, New York, 2005.
2. A. Muszynaka, P. Goldman, Chaotic responses of unbalanced rotor/bearing/stator system with looseness or rubs, ***Choas, Solitions and Fractals*** 5 (1995) 1683-1704.
3. F. Chu, Y. Tang, Stability and Non-linear responses of a rotor-bearing system with pedestal looseness, ***Journal of Sound and Vibration*** 241 (2001), 879-893.
4. Z. Ji , J. W. Zu, Method of multiple scales for vibration analysis of rotor-shaft systems with non-Linear bearing pedestal model, ***Journal of Sound and Vibration*** 218 (2) (1998), 293-305.
5. H. Ma, X. Zhao, Y Teng, et al, Analysis of dynamic characteristics for a rotor system with pedestal looseness. ***Shock and vibration*** 18 (2011), 13-27.
6. F. Ehrich, High-order subharmonic response of high-speed rotors in bearing clearance, ***Journal of Vibration Acoustics Stress and Reliability in Design-Transactions of the ASME*** 110 (1988) 9–16.
7. D. Childs, Fractional-frequency rotor motion due to nonsymmetric clearance effects, ***Journal of Engineering for Power*** 104 (1982) 533-541.
8. W. Zhang, G. Meng, et al, Nonlinear dynamics of a rub-impact micro-rotor system with scale-dependent friction model, ***Journal of Sound and Vibration*** 309 (2008) 756–777.
9. F. Chu, Z. Zhang, Bifurcation and Chaos in a Rub-Impact Jeffcott Rotor System, ***Journal of Sound and Vibration*** 210(1) (1998) 1-18.
10. S. Popprath, H. Ecker. Nonlinear dynamics of a rotor contacting an elastically suspended stator, ***Journal of Sound and Vibration*** 308 (2007) 767–784.

11. H. Nelson, J. Mcvaugh, The dynamics of rotor-bearing systems using finite elements, ***ASME Journal of Engineering for Industry*** 98(2) (1976) 593–600.
12. J. Jing, G. Meng, Y Sun, et al, On the oil-whipping of a rotor-bearing system by a continuum model, ***Applied Mathematical Modelling*** 29 (2005) 461-475.
13. Q. Han, Z. Zhang, B. Wen, Periodic motions of a dual-disc rotor system with rub-impact at fixed limiter, ***Journal of Mechanical Engineering Science*** 222 (2008) 1935-1946.
14. H. Ma, X. Tai, J. Sun, et al, Analysis of dynamic characteristics for a dual-disk rotor system with single rub-impact, ***Advanced Science Letters*** 4 (2011), 2782-2789.
15. P. Pennacchi, N. Bachschmid, E. Tanzi, Light and short arc rubs in rotating machines: Experimental tests and modeling, ***Mechanical Systems and Signal Processing*** 23 (2009) 2205-2227.
16. S. Chen, M. Geradin, Finite element simulation of non-linear transient response due to rotor-stator contact, ***Engineering Computations*** 14(6) (1997) 591-603.
17. A. Chavez, H. Ulbrich, L. Ginzinger, Reduction of contact forces in a rotor-stator-system in case of rubbing through active auxiliary bearing, ***Shock and Vibration*** 13(2006) 505-518.
18. L. Ginzinger, H. Ulbrich, Simulation and experiment of a rotor with unilateral contacts and active elements, ***IUTAM Symposium on Emerging trends in rotor dynamics*** (2011) 373-385.
19. L. Ginzinger, H. Ulbrich, Control of rubbing rotor using an active auxiliary bearing, ***Journal of Mechanical Science and Technology*** 21(2007) 851-854.
20. M. Sahinkaya, A. Abulrub, P. Keogh, et al, Multiple sliding and rolling contact dynamics for a flexible rotor/magnetic bearing system, ***IEEE/ASME Transactions on Mechatronics*** 12(2) (2007) 179-189.
21. S. Roques, M. Legrand, et al, Modeling of a rotor speed transient response with radial rubbing, ***Journal of Sound and Vibration*** 329 (2010) 527-546.
22. S. Roques, M. Legrand, et al, Development of beam-to-beam contact detection algorithms for rotor-stator rubbing application, Proceedings of *IDETC/CIE* 2007-21st ASME Biennial Conference on Mechanical Vibration and Noise, Las Vegas, Nevada, 2007.
23. T Patel, A Darpe, Vibration response of a cracked rotor in presence of rotor-stator rub, ***Journal of Sound and Vibration*** 317 (2008) 841–865.
24. G.Chen, C. Li, D. Wang. Nonlinear dynamic analysis and experiment verification of rotor-ball bearings-support-stator coupling system for aeroengine with rubbing coupling faults, ***Journal of Engineering for Gas Turbines and Power*** 132 (2010) 022501-1: 022501-9.
25. D. Xu, A new node-to-node approach to contact/impact problems for two dimensional elastic solids subject to finite deformation. PhD Thesis, The University of Illinois at Urbana-Champaign, 2008.
26. J. Simo, T. Laursen, An augmented Lagrangian treatment of contact problems involving friction, ***Computers and structures*** 42(1) (1992) 97-116.
27. T. Laursen, Computational Contact and Impact Mechanics: Fundamentals of Modeling Interfacial Phenomena in Nonlinear Finite Element Analysis, Springer, Berlin, 2003
28. K. Bathe, E. Wilson, Numerical methods in finite element analysis, Prentice-Hall, Inc., New Jersey, 1976.
29. H. Ma, X. Tai, J. Sun, et al. Analysis of dynamic characteristics for a dual-disk rotor system with single rub-impact, ***Advanced Science Letters*** 4 (2011) 2782-2789.

 ISSN 2572-4975 (Print), 2572-4991 (Online)